RSC Advances

PAPER

View Article Online
View Journal | View Issue



Cite this: *RSC Adv.*, 2022, **12**, 13511

# Prospective application of phosphorylated carbon nanofibers with a high adsorption capacity for the sequestration of uranium from ground water

V. Dhanya, Balasubramanian Arunraj and N. Rajesh *

Received 29th March 2022
Accepted 21st April 2022

DOI: 10.1039/d2ra02031a

rsc.li/rsc-advances

In this study carbon nanofibers (CNF) were phosphorylated by using *ortho*-phosphoric acid and applied for adsorptive remediation of uranium from water. The phosphorylated carbon nanofibers (PCNF) showed 96% removal of uranium as compared to 79% by CNF. The adsorption data from batch adsorption studies fitted well with the Langmuir model and a maximum adsorption capacity of 512.8 mg $g^{-1}$ was obtained at pH 6.0 while the adsorption followed pseudo second order kinetics. A detailed characterisation of the adsorbent has been carried out using various analytical and spectroscopic tools. The application of the adsorbent to ground water samples exhibited promising results even in the presence of other interfering cations and anions which is imperative considering the toxic effects of uranium in ground water.



## 1. Introduction

The need for viable, low-carbon and clean energy has significantly enhanced the quest for an alternative, sustainable and green energy source worldwide. Nuclear energy has already been proved to be an efficacious option and as per the data published by the World Nuclear Association in 2020,[1] it has contributed over 10% of electricity produced globally from 440 nuclear reactors. In India the nuclear energy share is about 3.1% generated from its 22 working nuclear reactors under the aegis of the Department of Atomic Energy, India.[2] Uranium, being the key element in nuclear fuel, is explored and extracted from its ores and later converted to metallic/oxide form suitable for use in a nuclear fission reactor. Uranium mining and ore processing, spent-fuel treatment, and radionuclide production in medical, industrial and research fields can contribute to contamination of water bodies.[3] Contamination of ground water by nitrates and phosphates released from chemical fertilizers used in agriculture has led to leaching of uranium from rocks and aquifers. $U^{4+}$ (uranous) & $U^{6+}$ ($UO_2^{2+}$, uranyl) are the two major oxidation states of uranium in nature. The uranyl species is soluble in water and migrates resulting in contamination of aqueous systems. Slight changes in the aqueous environment can lead to dissolution, migration and precipitation of uranium resulting in severe water pollution. Through pH 7–10, stable and highly mobile carbonate complexes of uranium are formed which extend throughout the food chain.[4] The World Health Organization (WHO) recommended the permissible limit of uranium in drinking water to be 30 μg $L^{-1}$ considering its chemical toxicity and radioactivity. Recent reports show widespread uranium contamination in ground water across many states in India much above the maximum permissible limits stipulated by the WHO and even the Atomic Energy Regulatory Board (AERB) limit of 60 μg $L^{-1}$.[5]

Various methods have been developed for the removal of uranium from aqueous solution including solvent extraction, membrane filtration, precipitation, electrocoagulation, photocatalysis, adsorption and biological treatments.[6–10] Among the known techniques, adsorption has been regarded as an economical and effective method for removing uranium from aqueous solutions. The ease of implementation, relatively low cost, wide adaptability and less generation of secondary waste attribute to its wide applicability. Numerous studies have been reported on the application of various materials as adsorbents for removing uranium from aquatic environments.[11]

A recent review on uranium remediation describes a wide variety of inorganic, organic, polymeric, carbon family and porous framework materials.[3] The inorganic materials include clay minerals,[12] metal oxides,[13] layered double hydroxides[14] and mesoporous silica[15] adsorbents. Organic polymers like ion exchange resins, cellulose, chitosan[16,17] *etc.* are reported to have good skeletal strength and adjustable physicochemical properties. Covalent, organic and metal–organic porous framework materials[18–21] possess high porosity, large surface area and ease of functionalisation. Zr based metal–organic frameworks (MOF) incorporated with phosphonate ligands have been reported to have ultrafast adsorption rate for uranium.[22] An adsorption capacity of 80 mg $g^{-1}$ from acidic medium was reported for uranium using MOF with phosphine oxide ligands.[23] $sp^2$ carbon-conjugated covalent organic frameworks were used for selective detection and extraction of uranium and was reported to have an exceptional $UO_2^{2+}$ adsorption capacity of 427 mg

*Department of Chemistry, Birla Institute of Technology and Science, Pilani, Hyderabad Campus, Jawahar Nagar, Hyderabad 500078, India. E-mail: nrajesh@hyderabad.bits-pilani.ac.in*

$g^{-1}$.[24] High adsorption kinetics, excellent selectivity and reusability of carbon family materials like activated carbon, mesoporous carbon, carbon nanotubes, nanofibers, and graphene oxide make them effective adsorbents for uranium remediation.[25–29] Carbon based nanomaterials have been widely used as adsorbents owing to the presence of different oxygenated functional groups and large specific surface area. High efficiency and simultaneous *in situ* monitoring of adsorption by luminescent mesoporous silica–carbon dots composite material has been reported.[30] Carbon superstructures fabricated through hydrothermal method exhibited reusability and scale up ability with an adsorption capacity of 197.7 mg $g^{-1}$ for uranium.[31]

Among the carbonaceous materials, carbon nanofibers are found to be versatile adsorbents due to high porosity, low density and ease of functionalisation.[32,33] Still only a few studies have been reported with carbon nanofibers as adsorbents for uranium. Yubing Sun *et al.* reported a maximum adsorption capacity of 125 mg $g^{-1}$ at pH 4.5 for carbonaceous nanofiber with good recyclability and recoverability.[34] Hollow tubular carbon nanofibers functionalised with carboxyl and sulphonic groups was reported to have maximum adsorption capacities of 1928.59 mg $g^{-1}$ and 1827.57 mg $g^{-1}$ respectively.[35] Phosphorylation is found to be effective for adsorption of uranium due to the inherent oxophilic nature of the metal ion. Carboni *et al.* reported phosphoric acid functionalised mesoporous carbon to have better adsorption capacity compared to amidoxime and carboxyl groups with a maximum sorption capacity of 97 mg $g^{-1}$ sorbent in acidic water and 67 mg $g^{-1}$ sorbent in artificial water.[36] Phosphoryl functionalised chitosan,[37] mesoporous carbon,[38] mesoporous silica,[39] graphene oxide,[40] carbon aerogel,[41] cellulose nanofiber,[42] luffa rattan activated carbon,[43] hyper cross-linked polymers,[44] iron doped ZIF[45] have been used for uranium adsorption.

In this work phosphorylated carbon nanofibers were prepared and used for the first time for adsorption of uranium from water. An exhaustive characterisation of the adsorbent using SEM, EDX, FTIR, XPS, XRD, BET and the various parameters like pH, kinetics and thermodynamics of the adsorption process are discussed in detail. The batch adsorption data is fitted with various isotherm models and a maximum adsorption of 512.8 mg $g^{-1}$ has been obtained using Langmuir model. The application of the adsorbent to ground water samples has been discussed as such reports are scarce. A description on the influence of the anions and cations usually present in ground water on the adsorption of uranium has also been given.

# 2. Experimental

## 2.1. Materials and methods

Graphitized, iron free carbon nanofibers (CNF) was obtained from Sigma Aldrich, *ortho*-phosphoric acid, $HNO_3$, NaOH were obtained from Merck India and ammonium dihydrogen phosphate was obtained from EMerck, Germany. For all dilutions, Millipore water was used. Stock solution of uranium (2000 mg $L^{-1}$) was prepared using $UO_2(NO_3)_2 \cdot 6H_2O$ purchased from Sisco Research Laboratories (SRL), India.

Fluorescence enhancing buffer was prepared by dissolving 250 g of ammonium dihydrogen phosphate in 500 mL Milli-Q water followed by addition of 60 mL *ortho*-phosphoric acid and making up to 1000 mL.

## 2.2. Quantification of uranium by spectrofluorimetry

Spectrofluorimetry[46] is a highly sensitive method for quantification of uranium in aqueous solutions. Although the absorption spectrum of uranium spreads from 200 to 420 nm, the excitation wavelength chosen for this study was 300 nm owing to its high intensity and relatively lesser quenching effects. The measurements of fluorescence were done at 516 nm, it being the most intense peak among the three distinct peaks at 490 nm, 516 nm and 540 nm characteristic of uranium fluorescence spectrum. A 40% (v/v) of the fluorescence enhancing buffer was maintained in all solutions used for uranyl fluorescence measurement. A steady state spectrofluorimeter model Fluorolog of HORIBA, Japan was used for all fluorescence measurements. All the solutions were equilibrated to 20 °C prior to fluorescence intensity measurement.

## 2.3. Synthesis of phosphorylated carbon nanofiber (PCNF)

Commercially obtained carbon nanofibers were heated with *ortho*-phosphoric acid (50% v/v) at 150 °C for 8 h on a hot plate. Further it was filtered, washed with deionised water for six times and dried in hot air oven at 110 °C for 24 h to obtain a dry powder of PCNF.

## 2.4. Characterization of adsorbents

The FT-IR spectra of adsorbents were recorded in the range 400–4000 $cm^{-1}$ using Jasco FT-IR 4200 model spectrophotometer. 1.0 mg of adsorbent was mixed with 100.0 mg spectroscopic grade potassium bromide to record the IR spectra. Apreo LoVac, FEI scanning electron microscope coupled with an EDX analysis system (Oxford X-Max) was used for surface analysis and elemental mapping of the adsorbents. X-ray diffraction pattern was recorded using Rigaku Ultima-IV X-ray diffractometer using Cu-K$\alpha$ radiation (1.5405 Å). K-Alpha, Thermo Fisher Scientific XPS instrument with aluminium monochromator was used to identify the oxidation states of uranium on the sorbents. The zeta potential of the adsorbent was measured using a zetasizer (Malvern Zetasizer Nano ZS) at varying pH values. Surface area, pore size and pore volume of the adsorbents were measured using BET (Microtrac Bel; BELSORP mini II).

## 2.5. Sorption experiments

$UO_2(NO_3)_2 \cdot 6H_2O$ was dissolved in Millipore water to prepare a stock solution of 2000 mg $L^{-1}$ of uranium and solutions of concentrations 2, 5, 10, 20, 50, 100, 200, 300, 400 and 500 mg $L^{-1}$ were prepared by serial dilution for isotherm study at room temperature. The pH of adsorption was optimized at 6.0 by using 0.1 M NaOH and 0.1 M $HNO_3$ solutions with an initial concentration of 10 mg $L^{-1}$ of uranium. 10 mg of sorbent was added to 20 mL of uranium solutions of varying concentrations and were agitated for 1 hour at 30 °C and 120 rpm for

attaining equilibrium in an orbital incubator shaker (Bio Technics, India). The solutions were then filtered using (Whatman 45) filter paper. The adsorption on to the filter paper and any precipitation at pH 6 were checked using uranium solution without adsorbent in the control experiments and was found to be minimal. The uranium concentration before and after adsorption was determined using spectrofluorimeter which was calibrated using a series of standards containing 0.1, 0.5, 1.0, 5.0 mg $L^{-1}$ uranium maintaining 10 mL fluorescence enhancing buffer in 25 mL solution.

The percentage removal of uranium was calculated using the eqn (1)

$$U(\text{removal})\% = \frac{C_0 - C_f}{C_0} \times 100 \quad (1)$$

And the equilibrium adsorption capacities ($q_e$) were calculated using eqn (2)

$$q_e = \frac{(C_0 - C_e)V}{m} \quad (2)$$

where $C_0$, $C_f$ and $C_e$ are the initial, final and equilibrium concentrations (mg $L^{-1}$) of U(VI) respectively, $V$ is the volume of solution (L) and $m$ is the mass of adsorbent (g) used.

The experimental data was fitted with Langmuir, Freundlich and Temkin isotherm models.

# 3. Results and discussion

## 3.1. Preparation of the adsorbent

Phosphorylation of the commercially obtained CNF was carried out separately using concentrated 85% $H_3PO_4$ at room temperature, 50% $H_3PO_4$ at 50 °C and 50% $H_3PO_4$ at 150 °C. The material prepared after treatment with concentrated $H_3PO_4$ was sticky and difficult to be dried into a powdery form. Moreover, it was highly acidic even after many cycles of washing with distilled water. Although the material obtained after phosphorylation at 50 °C using 50% $H_3PO_4$ was powdery, the adsorption capacity exhibited was less than 50%. Whereas, the adsorbent used in this study synthesized with 50% $H_3PO_4$ at 150 °C showed excellent adsorption ability towards uranium from aqueous solution.

## 3.2. Characterization of the adsorbent

**3.2.1. SEM and EDX analysis.** The surface morphology and elemental distribution of the native CNF, PCNF and uranium adsorbed PCNF (PCNFU) were studied using SEM imaging and EDX (Fig. 1). The images conveyed that the basic cylindrical, hollow tubular structure of the nanofibrils did not change much after functionalization and adsorption of the metal.[47] Nevertheless, the average diameter of the functionalized fibers (117 nm) is found to be more than that of the native one (109 nm) which could be attributed to the attached phosphate groups on the surface. Elemental mapping revealed homogeneous distribution of phosphorous on the surface of the adsorbent. The weight% of oxygen increased in the functionalized adsorbent indicating the introduction of phosphate moieties on its surface (Table 1).

**3.2.2. XPS analysis.** The binding energies and elemental characteristics of PCNF before and after adsorption were compared to give insights on the mechanistic interactions of uranium with the adsorbent (Fig. 2). In carbon 1s spectrum the peaks at 284.9 and 284.8 eV correspond to C–C, at 284.3 eV to C=C and peaks at 285.8 and 285.5 eV to C–OH for PCNF and PCNFU respectively.[48] The characteristic peaks $2p_{3/2}$ and $2p_{1/2}$

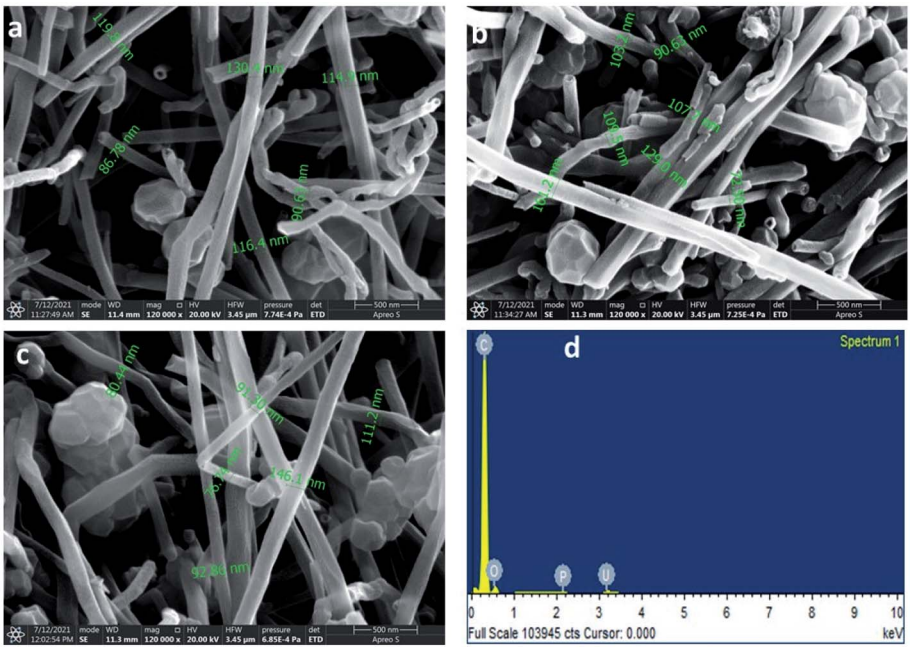


Fig. 1 SEM images of (a) CNF, (b) PCNF, (c) PCNFU, (d) EDX spectrum of PCNFU.

Table 1 Elemental composition of CNF, PCNF and PCNFU

| | Weight (%) [EDX analysis] | | | | Weight (%) [XPS analysis] | | | |
|---|---|---|---|---|---|---|---|---|
| Material | C | O | P | U | C | O | P | U |
| CNF | 92.5 | 7.5 | — | — | 76.28 | 23.72 | — | — |
| PCNF | 89.9 | 9.6 | 0.5 | — | 74.94 | 23.48 | 1.58 | — |
| PCNFU | 88.4 | 9.9 | 0.2 | 1.5 | 71.14 | 26.82 | 1.40 | 0.64 |

were obtained for P spectrum and the shift in binding energies from 134.5 to 133.8 eV for $2p_{3/2}$ and that of $2p_{1/2}$ from 136.3 to 134.8 eV indicate the electron density difference around P after adsorption. In the deconvoluted O 1s spectra the peaks at 532.08 and 531.9 eV correspond to P=O/P–O bond and peaks at 533.48 and 533.58 eV are assigned for P–O–C/C–O/C–O–C in PCNF and PCNFU respectively.[49] The XPS spectrum after adsorption showed two distinct peaks for U $4f_{7/2}$ at 382.08 eV and U $4f_{5/2}$ at 392.98 eV which confirms the presence of uranium in its hexavalent state.[50] These values are in agreement with the reported XPS studies by Ilton *et al.*[51] on different uranium oxidation states. However, the satellite peak obtained around 385 eV near U $4f_{7/2}$ peak could not be ascertained for the presence of U(IV) oxidation state. The shift in binding energy values after adsorption for O1s and P2p peaks could be correlated with the binding of the electropositive U(VI) ion with the negatively charged phosphate groups. Further, the increase in binding energy of U $4f_{7/2}$ peak from 381.3 for $OH/O^{2-}$ groups to 382.08 eV in PCNFU confirms interaction of uranium with $PO_4^{3-}$ anion with lower Lewis basicity.[52]

**3.2.3. FT-IR analysis.** Identification of the functional groups on CNF and PCNF were done using FT-IR (Fig. 3). The peaks around 3400 $cm^{-1}$ in both correspond to O–H stretching vibrations. C–H stretching peak was observed at around 2900 $cm^{-1}$ and at 1631 $cm^{-1}$ for C–H and C=C bonds.[37] Additional peaks obtained for PCNF at 1739 $cm^{-1}$,

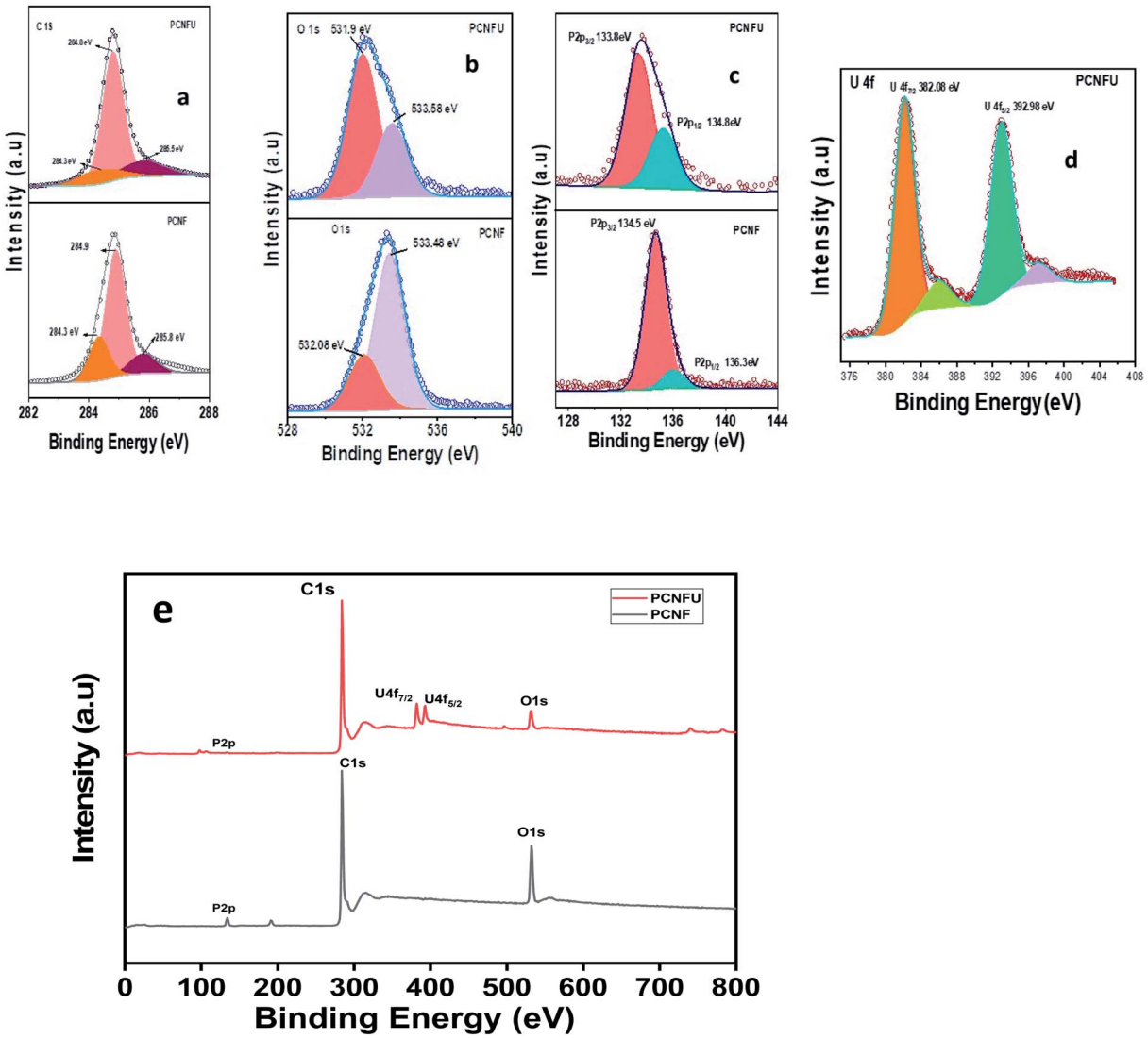


Fig. 2 High resolution XPS spectra of (a) C 1s, (b) O 1s, (c) P 2p and (d) U 4f of PCNF, PCNFU and (e) XPS survey scan spectra of PCNF and PCNFU.

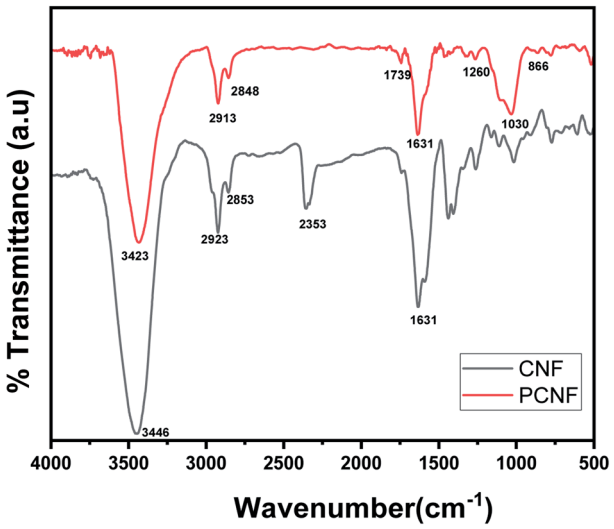


Fig. 3 FT-IR spectra of CNF and PCNF adsorbent materials.

1260 $cm^{-1}$, 1030 $cm^{-1}$ and 866 $cm^{-1}$ were assigned to C=O, P=O, C–O–P and P–O–C stretching vibrations respectively.[53] This confirms the successful modification of the nanofiber with phosphate group which is responsible for the efficient binding with U(VI).

**3.2.4. BET analysis.** The surface area, pore volume and pore diameter of native CNF, PCNF and uranium adsorbed PCNF are studied using BET. It was observed that the pore volume and diameter of the material increased after functionalization whereas the surface area remained almost constant (Table 2). This indicates that adsorption is favored mainly by the negatively charged surface phosphate groups. The data also reveals the mesoporous nature of the carbon nanofibers with a pore size within the range of 2.0 to 50 nm. The adsorption and desorption isotherms of CNF and PCNF are given in Fig. 4.

Table 2 BET parameters of CNF and PCNF materials

| BET parameters | CNF | PCNF |
|---|---|---|
| Total pore volume [$cm^3\ g^{-1}$] | 0.0756 | 0.0940 |
| Pore diameter [nm] | 14.489 | 18.403 |
| Surface area [$m^2\ g^{-1}$] | 21.788 | 21.703 |

**3.2.5. XRD analysis.** The X-ray diffractogram of CNF, PCNF and PCNFU was recorded (Fig. 5) and the data showed a peak corresponding to (002) plane at $2\theta = 26°$ in all which is typical for carbonaceous materials.[54] The pattern remained almost the same before and after adsorption indicating the structural stability of the material. The intensity of the peak is found to have increased after adsorption of metal ion.

### 3.3. Batch adsorption of uranium

**3.3.1. Effect of pH on adsorption.** Aqueous speciation is one of the key factors which decides the adsorption behaviour of U(VI). Different species of uranium is found in aqueous solution at varying pH. Adsorption of uranium from aqueous solution by CNF and PCNF was studied at varying pH ranging from 2 to 8 (Fig. 6a). Both the materials showed similar trend with a maximum adsorption at pH 6. The adsorption efficiency increased steadily with increase in pH, remaining almost constant in the range 5 to 7 and decreasing thereafter with increase in alkalinity. In acidic pH, uranium exists as free uranyl ions and the increased adsorption rate up to pH 7 could be attributed to the strong electrostatic interaction and resultant complexation between the positively charged $UO_2^{2+}$, $UO_2OH^+$ and $(UO_2)_2(OH)_2^{2+}$ and the negative surface groups on the adsorbent.[32] This observation can be justified by correlating the negative surface zeta potential values obtained for the adsorbent in the pH range 1.0 to 8.0 (Fig. 6b). The zeta potential became increasingly negative as the pH increased indicating the successive deprotonation of the phosphate groups which contributed to the enhanced adsorption capacity from pH 5.0 to 7.0. The sharp decrease of zeta potential could be attributed to the complete deprotonation of phosphate groups on the adsorbent surface at pH 6.0 and hence the maximum adsorption at this pH. The decrease in adsorption at alkaline pH could be associated with the electrostatic repulsion between the anionic species $((UO_2)_3(OH)_7)^-$ and $UO_2(OH)_3^-$ (formed as a result of hydrolysis) and the negative groups on the adsorbent.[55]

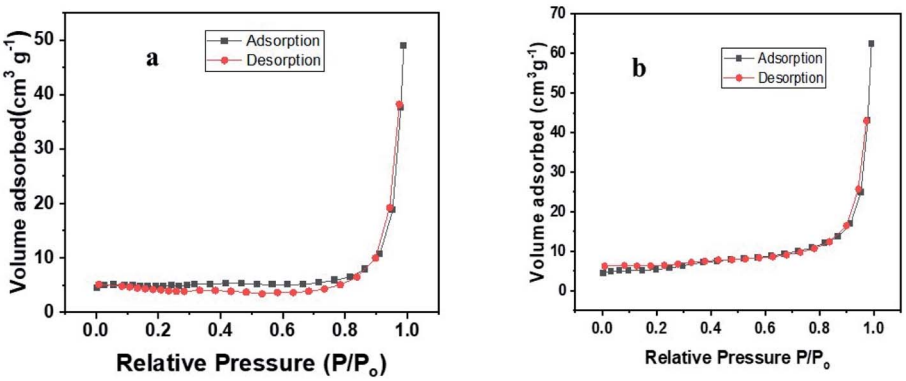


Fig. 4 $N_2$ adsorption and desorption isotherms of (a) CNF (b) PCNF.

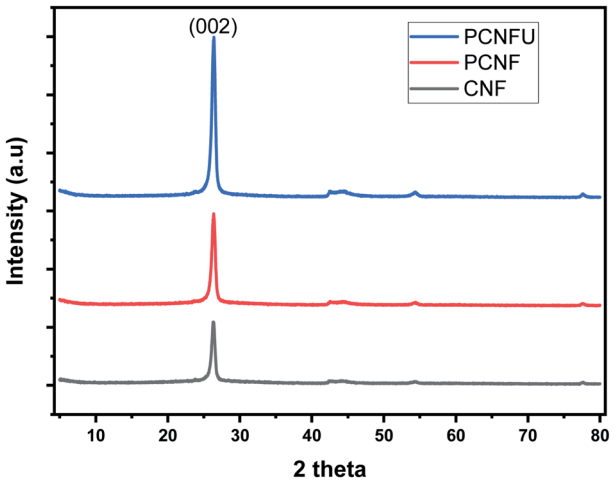


Fig. 5 XRD patterns of CNF, PCNF and PCNFU.

**3.3.2. Adsorption kinetics.** An understanding of the kinetic parameters of the adsorption process is crucial in assessing the reaction pathway and the mechanism of interaction between the adsorbate and the adsorbent. Kinetic study was performed with an initial uranium concentration of 55 mg $L^{-1}$ with an adsorbent dosage of 0.05 g in a sample volume of 0.05 L for a duration of two hours by withdrawing the aliquot of the sample at varying time intervals. The adsorption process attained equilibrium in sixty minutes. The data obtained from the kinetics of uranium adsorption on PCNF (Fig. 7) was investigated using pseudo-first order, pseudo-second order and intra-particle diffusion kinetic models as per the equations below:

$$\log(q_e - q_t) = \log q_e - (k_1/2.303)t \quad (3)$$

$$\frac{t}{q_t} = \frac{t}{q_e} + \frac{1}{k_2 q_e^2} \quad (4)$$

$$q_t = t^{1/2}k_i + C \quad (5)$$

where $k_1$ ($min^{-1}$) and $k_2$ (g $mg^{-1}$ $min^{-1}$) are the adsorption rate constants of the pseudo first order and pseudo second order kinetics respectively, $t$ (min) is the adsorption time, $q_e$ (mg $g^{-1}$) and $q_t$ (mg $g^{-1}$) are the quantities adsorbed at equilibrium and at time $t$ respectively. $k_i$ is the intra-particle diffusion rate constant (mg $g^{-1}$ $min^{-1/2}$) and $C$ is the intercept that gives information on the thickness of the boundary layer.

The pseudo first order model follows adsorption by diffusion through a boundary whereas the pseudo second order model describes adsorption involving surface chemisorption.[56] The adsorption of uranium by PCNF followed pseudo second order kinetics as indicated by the higher $R^2$ value as compared to pseudo first order as given in Table 3. Hence, it is concluded that the main control step of the adsorption rate is chemical reaction or chemical adsorption based on electron sharing.

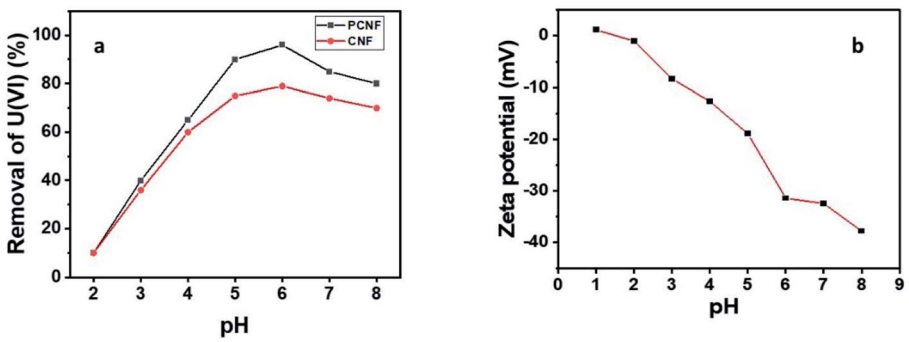


Fig. 6 (a) Effect of pH on adsorption of U(VI) by CNF and PCNF (b) zeta potential in the pH range 1–8 for PCNF.

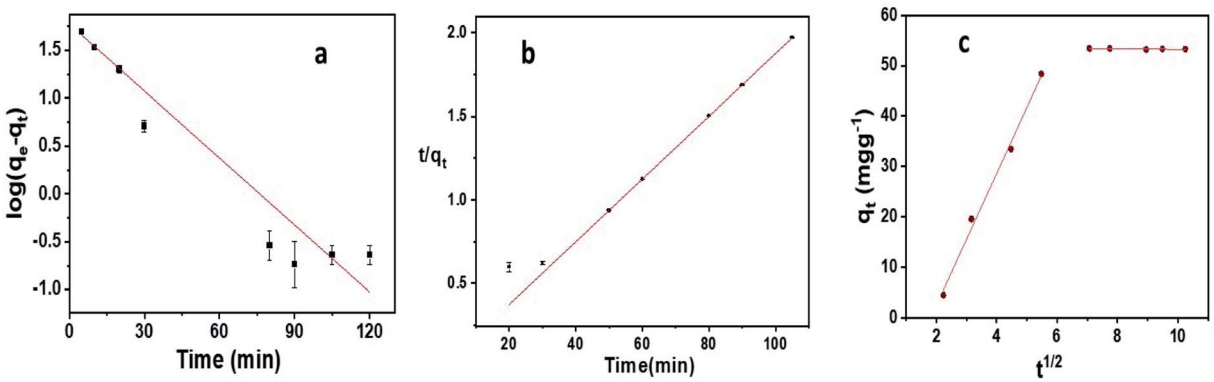


Fig. 7 Adsorption kinetics of U(VI) removal (a) pseudo-first-order, (b) pseudo-second-order and (c) intra-particle diffusion model.

Table 3 Kinetic parameters for the adsorption of U(VI) on PCNF

| Kinetics models | Kinetics parameters | Values |
|---|---|---|
| Pseudo-first-order | $k_1$ ($min^{-1}$) | 0.054 |
| | $q_{e1}$ (mg $g^{-1}$) | 59.422 |
| | $R^2$ | 0.948 |
| Pseudo-second-order | $k_2$ (g $mg^{-1}$ $min^{-1}$) | 0.314 |
| | $q_{e2}$ (mg $g^{-1}$) | 53.362 |
| | $R^2$ | 0.999 |
| Intra-particle diffusion | $C_1$ (mg $g^{-1}$) | −23.843 |
| | $k_{i1}$ (mg $g^{-1}$ $min^{-1/2}$) | 13.116 |
| | $R^2$ | 0.994 |
| | $C_2$ (mg $g^{-1}$) | 53.877 |
| | $k_{i2}$ (mg $g^{-1}$ $min^{-1/2}$) | −0.063 |
| | $R^2$ | 0.617 |

A straight line obtained on plotting metal ion adsorbed against the square root of contact time indicates intraparticle diffusion is rate limiting in the adsorption process. The linear trend observed for the plot indicates that film diffusion plays an important role in adsorption. The straight line not passing through the origin conveyed both intraparticle and film diffusions happen simultaneously on the adsorption of uranium by PCNF. The values given in Table 3 showed that the value of $k_{i1}$ was greater than that of $k_{i2}$ whereas the corresponding $C_1$ value was smaller than $C_2$. This is attributed to the faster adsorption resulting from the rapid external mass transfer in the initial phase of adsorption process. Upon saturation of the external surface, further adsorption on active sites on PCNF was assisted by diffusion of molecules in to the pores. The rate of adsorption decreased thereafter and reached equilibrium.[57]

**3.3.3. Adsorption isotherm studies.** Batch adsorption experiments showed 96% removal of uranium by PCNF compared to 79% by CNF from 20 mL solution containing 10 mg $L^{-1}$ uranium with an adsorbent dosage of 10 mg at pH 6. The experimental data obtained from adsorption using PCNF for varying uranium concentrations was fitted graphically to the linear Langmuir, Freundlich, and Temkin isotherm eqn (6)–(8).

$$\frac{C_e}{q_e} = \frac{C_e}{q_{max}} + \frac{1}{q_{max} K_L} \quad (6)$$

where $C_e$ is the equilibrium concentration of uranium in solution (mg $L^{-1}$), $q_e$ is the amount of U(VI) adsorbed at equilibrium per unit weight of the adsorbent (mg $g^{-1}$), $q_{max}$ is the maximum adsorption capacity for monolayer coverage (mg $g^{-1}$) and $K_L$ (L $mg^{-1}$) is the Langmuir constant which correlates with surface area and pore volume. From the linear Langmuir plot of $C_e/q_e$ against $C_e$, the slope gives $1/q_{max}$.[58]

$$\log q_e = \log K_F + \frac{1}{n} \log C_e \quad (7)$$

where $K_F$ is the adsorption capacity ($mg^{1-1/n}$ $g^{-1}$ $L^{1/n}$) and $n$ represents the Freundlich coefficient. $K_F$, $q_e$ and $n$ values are calculated through linear regression analysis.

$$q_e = \frac{RT}{b} \ln A + \frac{RT}{b} \ln C_e \quad (8)$$

where $b$ is Temkin constant associated with the heat of adsorption (J $mol^{-1}$), $A$ is the Temkin isotherm constant (L $g^{-1}$), $R$ is universal gas constant in SI unit and $T$ is the absolute temperature (kelvin).

A comparison of the results (Fig. 8) revealed that the data fitted well with Langmuir model with the highest $R^2$ value and a maximum adsorption capacity of PCNF is calculated to be 512.8 mg $g^{-1}$ at pH 6 (Table 4). This indicated the adsorption to be monolayer and homogeneous with the process occurring at

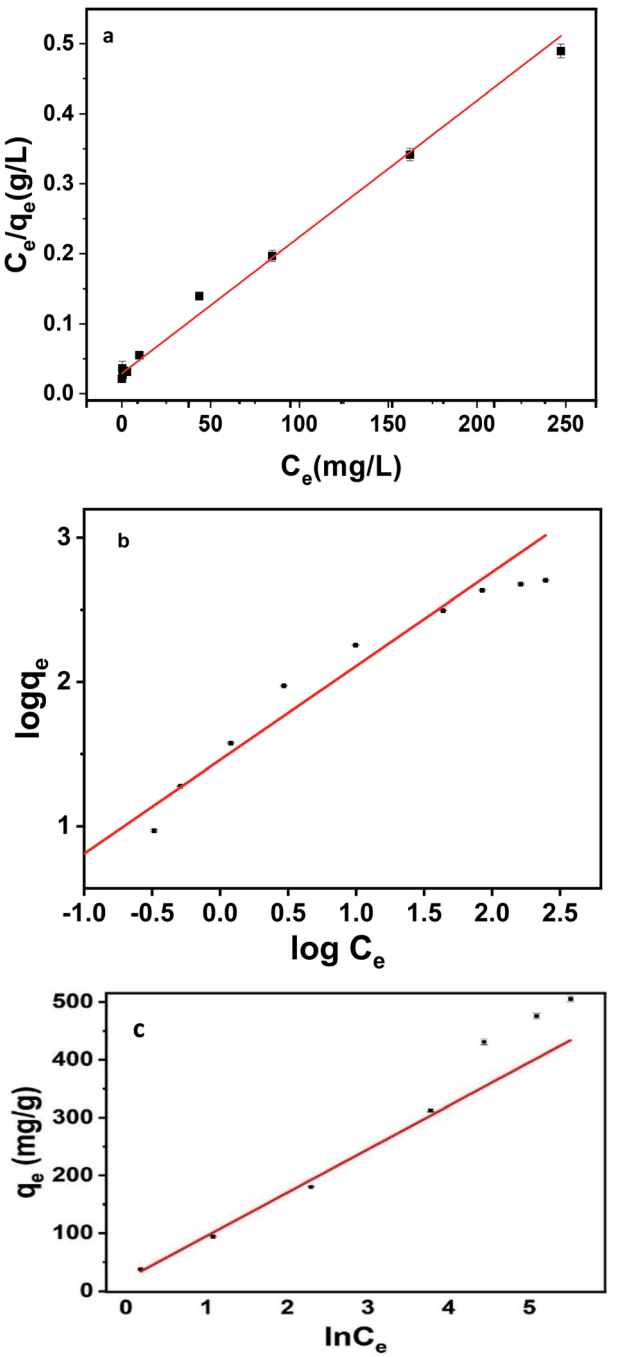


Fig. 8 Adsorption isotherms of uranium on PCNF (a) Langmuir isotherm, (b) Freundlich isotherm and (c) Temkin isotherm.

Table 4 Adsorption isotherm parameters for U(VI) adsorption on PCNF

| Isotherm models | Isotherm parameters | Values |
|---|---|---|
| Langmuir | $q_{max}$ (mg g$^{-1}$) | 512.82 |
| | $K_L$ (L mg$^{-1}$) | 1.00 |
| | $R^2$ | 0.99 |
| Freundlich | $K_F$ (mg$^{1-1/n}$ g$^{-1}$ L$^{1/n}$) | 27.08 |
| | $n$ | 1.63 |
| | $R^2$ | 0.96 |
| Temkin | $b_T$ (J mol$^{-1}$) | 33.02 |
| | $K_T$ (L g$^{-1}$) | 4.18 |
| | $R^2$ | 0.98 |

identical and equivalent sites. The separation factor $R_L$ given by eqn (9) indicates the nature of adsorption with $R_L = 1$ indicating linear, $R_L = 0$ as irreversible, $R_L > 1$ unfavorable and $0 < R_L < 1$ as favorable.[59] The calculated $R_L$ value for an initial uranium concentration of 20 mg L$^{-1}$ is 0.047 which confirms the favorable nature of adsorption on PCNF.

$$R_L = \frac{1}{1 + C_0 K_L} \quad (9)$$

The effectiveness of adsorption is also indicted by the $n$ value obtained from Freundlich plot. Values of $n$ from 1 to 10 indicate effective adsorption in general and the value of $n$ calculated as 1.63 for adsorption of uranium on PCNF showed the process to be highly efficient. The adsorption data was also fitted with Temkin model according to which adsorption process is characterized by distribution of binding energies evenly on the surface of the adsorbent till a maximum binding energy is reached.[60]

A comparison of the adsorption capacities reported recently for carbon-based materials has been given in Table 5. From this it is evident that phosphorylated carbon nanofibers exhibit excellent adsorption ability much better than many of the other carbonaceous materials. Also, the fact that the adsorption capacity was above 80% in the pH range of 5 to 8 with a maximum adsorption at pH 6 makes it a versatile material for removal of uranium from contaminated ground water samples.

**3.3.4. Thermodynamic study.** Temperature has an effect on adsorption process based on the mechanism involved. The diffusion rate of the sorbate through the layers and pores of the sorbent as well as the equilibrium capacity can vary with temperature.[61]

The thermodynamic state functions $\Delta H^\circ$ (kJ mol$^{-1}$), $\Delta G^\circ$ (kJ mol$^{-1}$) and $\Delta S^\circ$ (J mol$^{-1}$ K$^{-1}$) were determined using the linear form of van't Hoff eqn (10) and (11) plotted using the adsorption data at different temperatures.

$$\ln K_{eq} = \frac{-\Delta H^\circ}{R}\left(\frac{1}{T}\right) + \frac{\Delta S^\circ}{R} \quad (10)$$

$$\Delta G^\circ = -RT \ln K_{eq} \quad (11)$$

where $K_{eq}$ is the equilibrium constant obtained from the ratio of concentration of uranium ions on the adsorbent surface to that in the solution phase. The slope and intercept values of ln $K_{eq}$ against $1/T$ plot (Fig. 9) were used to calculate the enthalpy and entropy changes during adsorption. The adsorption process was found to be spontaneous as indicated by the negative $\Delta G^\circ$ values for each of the experimental temperatures. The enthalpy change of adsorption is found to be positive indicating adsorption process to be endothermic. Positive $\Delta S^\circ$ values suggest the increase in randomness on adsorption as a result of the exchange of mobile cations on adsorbent surface with the uranyl ions. The values are tabulated in Table 6.

### 3.4. Mechanism of interaction between uranium and the adsorbent

In aqueous solution varied species of uranium have been reported to be present between pH 2 to 8. At acidic pH, the $H^+$ ions present in solution compete with uranyl ions for the adsorbent sites. As the pH increases from 2 to 6 the successive deprotonation of PCNF makes the adsorbent surface more negative which is in conformity with the surface charge values obtained from zeta potential measurements, thus facilitating better adsorption of the metal ion species from solution. The maximum adsorption capacity of PCNF was achieved at pH 6 with the capacity nearly constant in the range of pH 5 to 7 and the predominant species reported at this pH include $UO_2^{2+}$ and the hydroxyl species like $UO_2OH^+$, $(UO_2)_2(OH)_2^+$ and $(UO_2)_3(OH)_5^+$.[62] Hence the excellent adsorption by PCNF could be due to the strong electrostatic interactions between the

Table 5 Comparison of adsorption capacity with a few recently reported carbon based adsorbents for remediation of uranium from water

| Adsorbent | $q_{max}$ (mg g$^{-1}$) | pH | References |
|---|---|---|---|
| Phosphorylated iron-doped ZIF-8 | 691.8 | 4.5 | 45 |
| Phosphate functionalised polyethylene | 173.8 | 8.2 | 61 |
| Magnesium functionalised ferro-metal–carbon composite | 118.5 | 5–6 | 64 |
| Phosphorylated hyper cross-linked polymers | 297.1 | 7.0 | 44 |
| Phosphorylated cellulose | 1550.0 | 6.0 | 42 |
| Phytic acid functionalised carbon nanomaterial | 552.4 | 5.0 | 54 |
| sp$^2$ carbon conjugated covalent organic frame work | 410.0 | 4.0 | 24 |
| Graphene oxide 3D mesoporous MOF nanocomposite | 416.7 | 6.2 | 18 |
| Phosphorylated luffa rattan activated carbon | 197.0 | 5.0 | 43 |
| Phosphorylated carbon nanofiber | 512.8 | 6.0 | This study |

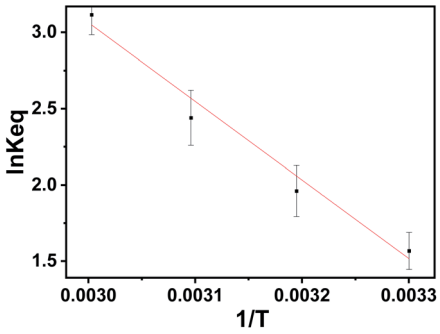


Fig. 9 Thermodynamics of adsorption of U(VI) through van't Hoff plot of ln $K_{eq}$ against 1/$T$.

Table 6 Thermodynamic parameters for the adsorption of U(VI) on PCNF

| Temperature (kelvin) | $\Delta H^0$ (kJ mol$^{-1}$) | $\Delta S^0$ (kJ mol$^{-1}$ K$^{-1}$) | $\Delta G^0$ (kJ mol$^{-1}$) | $R^2$ |
|---|---|---|---|---|
| 303 | 42.84 | 0.154 | −3.948 | 0.975 |
| 313 | | | −5.102 | |
| 323 | | | −6.553 | |
| 333 | | | −8.625 | |

oppositely charged phosphate groups on the surface of the adsorbent and these metal ion species in solution. Additionally, the information obtained from FTIR and XPS data also confirm the binding of phosphate on to the carbon nanofibers and the adsorption of uranium ions. The new peaks corresponding to the stretching vibrations of P=O at 1260 cm$^{-1}$, C–O–P at 1030 cm$^{-1}$ and P–O–C at 866 cm$^{-1}$ obtained for PCNF indicate the introduction of phosphate moiety on the surface of carbon nanofibers. The shift in binding energies obtained for O 1s and P 2p peaks confirm the binding of uranium on to the adsorbent through the oxygen atoms of phosphate groups. The decrease in binding energies from 134.6 to 133.7 eV for $2p_{3/2}$ and that of $2p_{1/2}$ from 136.3 to 134.8 eV on adsorption could be attributed to the increase in electron density near P atoms as a result of the decrease in electronegativity of oxygen atoms bound to metal ion. Further the adsorption followed pseudo second order kinetics and was found to be endothermic in nature confirming the chemical interactions between the phosphate groups and uranium ions. The probable interactions between uranyl species and PCNF could include coordination between the lone pairs of oxygen of P=O bond and electrostatic attraction between negatively charged oxygens as shown in Fig. 10.[63]

### 3.5. Desorption and regeneration of the adsorbent

Regeneration and reuse of the adsorbent material is essential for its economical application and also to comply with the green chemistry principles. Therefore, experiments were conducted to test the extent of desorption of U(VI) from PCNFU using 0.5 M $HNO_3$ solution. It was observed that the adsorbed U(VI) was desorbed almost completely (>98%) with single treatment of 0.5 M $HNO_3$. The recovered adsorbent was put to use for

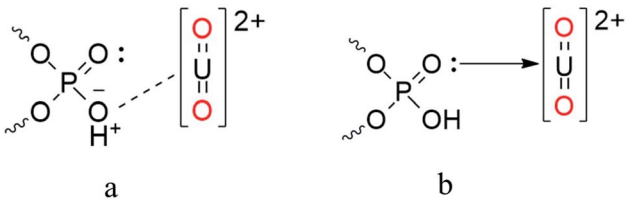


Fig. 10 Schematic interactions of uranyl ion and phosphate groups (a) electrostatic interaction (b) coordination.

multiple cycles ($n$ = 3) and found to be effectively adsorbing U(VI) although with decreased efficiency of 80% after the third adsorption–desorption cycle. Therefore, it is expected that the adsorbent PCNF can be used effectively for application to ground water samples with uranium contamination.

### 3.6. Selectivity of adsorbent to uranium

The selectivity of adsorbent to uranium was established in the presence of other divalent heavy metal ions (Fe, Cd, Co, Cr, Cu, Pb and V). Results obtained are given in Fig. 11. The removal efficiencies were found to be in the following order, U > Pb > Cu > Cd > Fe > Cr > Co > V at pH 6 using an adsorbent dosage of 20 mg. The high selectivity of uranium to PCNF could be attributed to the oxophilic nature of uranium and the high affinity of oxygen rich phosphate group to it. This is in agreement with the results obtained from XPS and FTIR studies. Interestingly the adsorption capacity of uranium is not influenced by the competitive adsorption of $Pb^{2+}$. Among the concomitant metal ions studied, vanadium showed least adsorption at the studied pH on PCNF even though it has been reported as a competitive ion in separation of uranium from sea water. This result indicates that PCNF could be a promising material for selective adsorption of uranium even from sea water containing vanadium.

### 3.7. Application to ground water samples

PCNF was applied to ground water samples collected from different drinking water sources in and around Hyderabad,

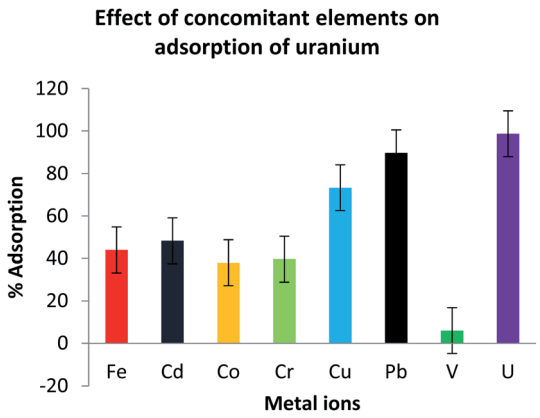


Fig. 11 Selectivity of PCNF to uranium over other ions at initial concentrations of 1.0 mg L$^{-1}$.

Table 7 Spike recovery of U(VI) in ground water samples and the multi-ions present in those samples

| Sample no. | U in sample (ng mL$^{-1}$) | U spiked (ng mL$^{-1}$) | U adsorbed (%) | pH | $Na^+$ (μg mL$^{-1}$) | $K^+$ (μg mL$^{-1}$) | $Ca^{2+}$ (μg mL$^{-1}$) | $Mg^{2+}$ (μg mL$^{-1}$) | $Cl^-$ (μg mL$^{-1}$) | $F^-$ (μg mL$^{-1}$) | $HCO_3^-$ (μg mL$^{-1}$) | $SO_4^{2-}$ (μg mL$^{-1}$) | $NO_3^-$ (μg mL$^{-1}$) |
|---|---|---|---|---|---|---|---|---|---|---|---|---|---|
| GW-1 | 5 | 1000 | 95 | 7.2 | 40 | 5 | 40 | 24 | 52 | 0.8 | 220 | 43 | 8 |
| GW-2 | 30 | 1000 | 87 | 7.5 | 100 | 5 | 104 | 53 | 183 | 2.2 | 590 | 131 | 13 |
| GW-3 | 36 | 1000 | 87 | 8.1 | 80 | 4 | 32 | 35 | 113 | 3.7 | 320 | 37 | 20 |
| GW-4 | 13 | 1000 | 92 | 7.8 | 129 | 2 | 108 | 19 | 167 | 1 | 213 | 100 | 15 |
| GW-5 | 2 | 1000 | 88 | 7.9 | 320 | 3 | 70 | 20 | 202 | 1.4 | 331 | 250 | 10 |
| GW-6 | 7 | 1000 | 90 | 7.2 | 228 | 2 | 78 | 20 | 163 | 1.3 | 294 | 100 | 22 |

India and were doped with uranium (1000 ng mL$^{-1}$) which is nearly 35 times higher than the permissible limits set by WHO (30 ng mL$^{-1}$). Water samples were analyzed for their major cations and anions and the data obtained is depicted in the Table 7. The adsorbent exhibited excellent sorption capacity (87–95%) in all the samples at the optimized pH. The variation in adsorption capacity can be attributed to the varying compositions of anionic and cationic species present in the chosen environmental samples. From Table 7 it is evident that with the increase in concentrations of complexing anions like $F^-$, $HCO_3^-$ there is a decrease in percentage of adsorption. As pH of all the samples are less than 8.3, the presence of $CO_3^{2-}$, a much better complexing anion, is ruled out. The selectivity of PCNF towards uranium in presence of larger concentration of cations like Na, K, Ca and Mg can be ascribed to the superior affinity and complexing ability of phosphate group towards uranium.[64]

## 4. Conclusions

A simple, rapid method for modification of carbon nanofibers through phosphorylation was optimized to obtain an enhanced adsorption capacity for U(VI) from aqueous systems. A detailed characterisation of the adsorbent revealed that the efficient capture of the metal ion could be attributed to the higher porosity of PCNF and the electrostatic interactions between the negatively charged phosphoryl group and U(VI) cation. The adsorption followed pseudo second order kinetics and was found to be endothermic in nature implying strong chemisorptive interactions. A maximum adsorption capacity of 512.8 mg g$^{-1}$ of adsorbent was obtained at pH 6.0. The adsorbent was used for removal of uranium from real ground water samples. An excellent adsorption ability as high as 87–95% was demonstrated even in samples having higher concentrations of bicarbonate and fluoride. Selectivity studies revealed the preferential adsorption of U over other concomitant divalent cations. Hence, the developed adsorbent is proved to be a promising material for remediation applications for uranium contaminated aqueous environment.

## Author contributions

Rajesh was instrumental in the conceptualization of the study. Dhanya performed all the experimental studies and characterizations related to adsorption. Arunraj was involved in the interpretation of data and overall presentation of the manuscript. All the authors concur towards their respective contributions.

## Conflicts of interest

The authors declare no conflict of interest.

## Acknowledgements

The authors thank the Central Analytical Laboratory, BITS Pilani, Hyderabad Campus, India for the analytical

characterisation. Dhanya V. thanks the support and encouragement of St. Francis College for Women, Hyderabad, India.



## Notes and references

1 *World Nuclear Performance Report 2020*, World Nuclear Association, U.K., **https://world-nuclear.org/information-library/current-and-future-generation/nuclear-power-in-the-world-today.aspx**, Report No. 2020/008, August.
2 **https://en.wikipedia.org/wiki/Nuclear_power_in_India**, accessed on 23rd February, 2022.
3 Y. Xie, C. Chen, X. Ren, X. Wang, H. Wang and X. Wang, *Prog. Mater. Sci.*, 2019, **103**, 180–234.
4 S. V. Gudkov, A. V. Chernikov and V. I. Bruskov, *Russ. J. Gen. Chem.*, 2016, **86**, 1531–1538.
5 R. M. Coyte, R. C. Jain, S. K. Srivastava, K. C. Sharma, A. Khalil, L. Ma and A. Vengosh, *Environ. Sci. Technol. Lett.*, 2018, **5**, 341–347.
6 P. D. Bhalara, D. Punetha and K. Balasubramanian, *J. Environ. Chem. Eng.*, 2014, **2**, 1621–1634.
7 J. Li and Y. Zhang, *Procedia Environ. Sci.*, 2012, **13**, 1609–1615.
8 I. A. Katsoyiannis and A. I. Zouboulis, *Desalin. Water Treat.*, 2013, **51**, 2915–2925.
9 B. Denis, G. Cote, H. Mokhtari, B. Courtaud, B. A. Moyer and A. Chagnes, *Chem. Rev.*, 2014, **114**, 12002–12023.
10 V. N. Salomone, J. M. Meichtry, G. Zampieri and M. I. Litter, *Chem. Eng. J.*, 2015, **261**, 27–35.
11 M. Gao, G. Zhu and C. A. Gao, *Energy Environ. Focus*, 2014, **3**, 219–226.
12 V. Tobilko, L. Spasonova, I. Kovalchuk, B. Kornilovych and Y. Kholodko, *Colloids Interfaces*, 2019, **3**, 41–52.
13 Z. Yu, Q. Li, J. Liao, Y. Zhang, L. Zhang and W. Zhu, *J. Alloys Compd.*, 2021, **868**, 159069.
14 S. Ma, L. Huang, L. Ma, Y. Shim, S. M. Islam, P. Wang, L. Zhao, S. Wang, G. Sun, X. Yang and M. G. Kanatzidis, *J. Am. Chem. Soc.*, 2015, **137**, 3670–3677.
15 D. Li, S. Egodawatte, D. I. Kaplan, S. C. Larsen, S. M. Serkiz and J. C. Seaman, *J. Hazard. Mater.*, 2016, **317**, 494–502.
16 C. Christou, K. Philippou, T. Krasia-Christoforou and I. Pashalidis, *Carbohydr. Polym.*, 2019, **219**, 298–305.
17 M. K. Sureshkumar, D. Das, M. B. Mallia and P. C. Gupta, *J. Hazard. Mater.*, 2010, **184**, 65–72.
18 A. Amini, M. Khajeh, A. R. Oveisi, S. Daliran, M. Ghaffari-Moghaddam and H. S. A. Delarami, *J. Ind. Eng. Chem.*, 2020, **93**, 322–332.
19 A. Yang, A. Z. Wang and Y. Zhu, *Sci. Rep.*, 2020, **10**, 19271.
20 X. Qin, W. Yang, Y. Yang, D. Gu, D. Guo and Q. A. Pan, *Inorg. Chem.*, 2020, **59**, 9857–9865.
21 B. Li, Q. Sun, Y. Zhang, C. W. Abney, B. Aguila, L. Wenbin and M. Shengqian, *ACS Appl. Mater. Interfaces*, 2017, **9**, 12511–12517.
22 W. Zhang, A. Bu, Q. Ji, L. Min, S. Zhao, Y. Wang and J. Chen, *ACS Appl. Mater. Interfaces*, 2019, **11**, 33931–33940.
23 W. Zhang, X. Dong, Y. Mu, Y. Wang and J. Chen, *J. Mater. Chem. A*, 2021, **9**, 16685–16691.
24 W. R. Cui, C. R. Zhang, W. Jiang, F. Li, R. Liang, J. Liu and J. Qiu, *Nat. Commun.*, 2020, **11**, 436.
25 X. Yang, Y. Wan, Y. Zheng, F. He, Z. Yu, J. Huang and B. Gao, *Chem. Eng. J.*, 2019, **366**, 608–621.
26 M. Mauter and M. Elimelech, *Environ. Sci. Technol.*, 2008, **42**, 5843–5859.
27 H. Guo, P. Mei, J. Xiao, X. Huang, A. Ishag and Y. Sun, *Chemosphere*, 2020, **278**, 130411.
28 W. A. Carter, T. M. Richard, S. Tomonori and D. Sheng, *Chem. Rev.*, 2017, **117**, 13935–14013.
29 S. Verma and K. Ki-Hyun, *Environ. Int.*, 2022, **158**, 106944.
30 Z. Wang, C. Xu, Y. Lu, F. Wu, Y. Gang, G. Wei, T. Sun and J. Chen, *ACS Appl. Mater. Interfaces*, 2017, **9**, 7392–7398.
31 B. Hana, E. Zhang, G. Cheng, L. Zhang, D. Wang and X. Wang, *Chem. Eng. J.*, 2018, **338**, 734–744.
32 H. W. Liang, L. Wang, P. Y. Chen, H. T. Lin, L. F. Chen, D. He and S. H. Yu, *Adv. Mater.*, 2010, **22**, 4691–4695.
33 H. W. Liang, Q. F. Guan, L. F. Chen, Z. Zhu, W. J. Zhang and S. H. Yu, *Angew. Chem., Int. Ed.*, 2012, **51**, 5101–5105.
34 Y. Sun, Z. Wu, X. Wang, C. Ding, S. Yu, W. Cheng and X. Wang, *Environ. Sci. Technol.*, 2016, **50**, 4459–4467.
35 M. Ahmad, K. Yang, L. Li, Y. Fan, T. Shah, Q. Zhang and B. Zhang, *ACS Appl. Nano Mater.*, 2020, **3**, 6394–6405.
36 M. Carboni, C. W. Abney, M. L. Kathryn, T. Pashow, J. V. Escoto and W. Lin, *Ind. Eng. Chem. Res.*, 2013, **52**, 15187–15197.
37 A. M. A. Morsy, *Environ. Technol. Innovation*, 2015, **4**, 299–310.
38 Y. Zou, X. Cao, X. Luo, Y. Liu, R. Hua, Y. Liu and Z. J. Zhang, *J. Radioanal. Nucl. Chem.*, 2015, **306**, 515–525.
39 G. Xue, F. Yurun, M. Li, G. Dezhi, J. Jie, Y. Jincheng, S. Haibin, G. Hongyu and Z. Yujun, *Appl. Surf. Sci.*, 2017, **402**, 53–60.
40 C. Yawen, W. Chunfang, L. Zhiyong, Z. Linjuan, C. Lanhua, W. Jianqiang, W. Xiangke, Y. Shitong and W. Shuao, *Environ. Sci.: Nano*, 2017, **4**, 1876.
41 Z. Zhang, Z. Dong, X. Wang, D. Ying, X. Cao, Y. Wang, R. Hua, H. Feng, J. Chen, Y. Liu, B. Hu and X. Wang, *Chem. Eng. J.*, 2019, **370**, 1376–1387.
42 J. Lehtonen, J. Hassinen, A. A. Kumar, L. S. Johansson, R. Mäenpa, N. Pahimanolis, T. Pradeep, O. Ikkala and O. J. Rojas, *Cellulose*, 2020, **27**, 10719–10732.
43 Z. Yanan, Y. Tianzhen, W. Yun, Z. Limin and L. Zhirong, *J. Radioanal. Nucl. Chem.*, 2021, **327**, 1267–1275.
44 Y. Tian, L. Liu, F. Ma, X. Zhu, H. Dong, C. Zhang and F. Zhao, *J. Hazard. Mater.*, 2021, **419**, 126538.
45 J. Pei, Z. Chen, Y. Wang, B. Xiao, Z. Zhang, X. Cao and Y. Liu, *J. Solid State Chem.*, 2022, **305**, 122650.
46 S. Maji, S. Kumar and K. Sundararajan, *J. Radioanal. Nucl. Chem.*, 2021, **329**, 1061–1066.
47 P. Tatarko, V. Puchy, J. Dusza, J. Morgiel, Z. Bastl and J. Mihaly, *Kovove Mater.*, 2010, **48**, 379–385.
48 D. J. Morgan, *C*, 2021, **7**, 51.
49 S. Campisi, F. J. S. rujillo, D. Motta, T. E. Davies, N. Dimitratos and A. Villa, *C*, 2018, **4**, 48.
50 J. F. Moulder, W. F. Stickle, P. E. Sobol and K. D. Bomben, *Handbook of X-ray Photoelectron Spectroscopy: A Reference*

*Book of Standard Spectra for Identification and Interpretation of XPS Data*, Perkin-Elmer Corp., Physical Electronics Division, Eden Prairie, 1995.

51 E. S. Ilton and P. S. Bagus, *Surf. Interface Anal.*, 2011, **43**, 1549–1560.

52 M. Schindler, F. C. Hawthorne, M. S. Freund and P. C. Burns, *Geochim. Cosmochim. Acta*, 2009, **73**, 2471–2487.

53 C. Luhrs, M. Moberg, A. Maxson, L. Brewer and S. Menon, *Inorganics*, 2014, **2**, 211–232.

54 L. Li, R. Ma, T. Wen, P. Gu, S. Zhang, M. Zheng, X. Wu, X. Zhang, T. Hayat and X. Wang, *Sci. Total Environ.*, 2019, **694**, 133697.

55 L. Dolatyari, M. R. Yaftian and S. J. Rostamnia, *Environ. Manage.*, 2016, **169**, 8–17.

56 A. Pholosi, E. B. Naidoo, A. E. Ofomaja and S. Afr, *J. Chem. Eng.*, 2020, **2**, 39–55.

57 A. A. Aryee, F. M. Mpatani, A. N. Kani, E. Dovi, R. Han, Z. Li and L. Qu, *Environ. Sci. Pollut. Res.*, 2020, **27**, 40316–40330.

58 B. Arunraj, T. Satvika, V. Rajesh and N. Rajesh, *Sep. Sci. Technol.*, 2019, **54**, 1620–1631.

59 M. A. Al-Ghouti and D. A. Da'ana, *J. Hazard. Mater.*, 2020, **393**, 122383.

60 A. O. Dada, A. P. Olalekan, A. M. Olatunya and O. Dada, *IOSR-JAC*, 2012, **3**, 38–45.

61 D. Shao, Y. Li, X. Wang, S. Hu, J. Wen, J. Xiong, A. M. Asiri and H. M. Marwani, *ACS Omega*, 2016, **2**, 3267–3275.

62 P. Lyu, G. Wang, B. Wang, Q. Yin, Y. Li and N. Deng, *Appl. Clay Sci.*, 2021, **209**, 106146.

63 U. Pinaeva, N. Ollier, O. Cavani, E. Balanzat, M. Al-Sheikhly, T. L. Wade and M. C. Clochard, *Sci. Rep.*, 2020, **10**, 5776.

64 R. Wu, Z. Han, H. Chen, G. Cao, T. Shen, X. Cheng and Y. Tang, *ACS ES&T Water*, 2021, **1**, 980–990.